scientific reports

Check for updates

OPEN

Genome-wide analysis of quorum sensing regulon in marine fish pathogen *Vibrio scophthalmi*

Bokyung Seok[1], Myoung Sug Kim[2] & Byoung Sik Kim[1]✉

Opportunistic fish pathogen *Vibrio scophthalmi* frequently infects olive flounder and turbot, which are primary marine species cultured for seafood production in Far East Asia. These infections cause substantial yield reductions and significant economic losses. Although quorum sensing (QS) genes were previously reported in *V. scophthalmi*, the impacts of QS on genome-wide gene expression and consequent behaviors and physiological traits have remained largely unexplored. In this study, we conducted genomic and transcriptomic analyses to uncover the global regulatory network governed by $LuxR_{Vs}$, a QS master regulator in *V. scophthalmi*. By comparing the wild-type strain and a $luxR_{Vs}$ deletion mutant strain, we found that $LuxR_{Vs}$ positively regulates biosynthetic genes for poly-hydroxyalkanoate (PHA) while negatively controlling genes for biofilm formation. Quantification of intracellular PHAs and biofilm biomass on borosilicate tubes confirmed these results. Gene set enrichment analyses further demonstrated that $LuxR_{Vs}$ also governs genes related to osmoprotection and defense against reactive oxygen species. Overall, these findings indicate that $LuxR_{Vs}$ acts as a global transcriptional regulator, controlling a wide range of physiological processes in *V. scophthalmi*. Targeting $LuxR_{Vs}$ could therefore be a promising strategy for improving seafood production by disrupting diverse physiological and pathogenic traits in this fish pathogen.

Keywords Quorum sensing, *Vibrio scophthalmi*, Fish pathogen, Seafood production, LuxR regulon

Abbreviations

AB	Autoinducer bioassay medium
ABC	ATP-binding cassette
AI	Autoinducer
c-di-GMP	Cyclic bis-(3', 5')-dimeric guanosine monophosphate
CDS	Coding sequence
DEG	Differentially expressed gene
GO	Gene ontology
GTP	Guanosine 5'-triphosphate
IMP	Inosine 5'-monophosphate
KEGG	Kyoto encyclopedia of genes and genomes
HCD	High cell density
LB	Luria-Bertani medium
LBS	LB medium supplemented with sodium chloride
LCD	Low cell density
$LuxR_{Vs}$	*Vibrio scophthalmi* LuxR
MSHA	Mannose-sensitive hemagglutinin
PHA	Poly-hydroxyalkanoate
qRT-PCR	quantitative Real-Time PCR
QS	Quorum sensing
ROS	Reactive oxygen species
TMM	Trimmed mean of M-values
VPS	*Vibrio* polysaccharide
WT	Wild-type
MT	Mutant

[1]Department of Food Science and Biotechnology, College of Engineering, Ewha Womans University, Seoul 03760, South Korea. [2]Pathology Research Division, National Institute of Fisheries Science, Busan 46083, South Korea. ✉email: b.kim@ewha.ac.kr

The ongoing climate crisis significantly impacts on sustainable food production. Limited land for agriculture and stock-farming further worsens the existing problem[1]. Therefore, various strategies for sustainable food supplies are under intensive investigation, such as meat alternatives and cultured meats[2]. However, given that approximately 17% of edible meats currently come from various seafoods, it is crucial to reconsider the potential of aquaculture as a reliable alternative to land-derived food production. In fact, it has been predicted that global seafood production will increase from 59 megatons to 80–103 megatons by 2050[3].

Among the various species cultivated in aquaculture, the olive flounder (*Paralichthys olivaceus*) holds a significant position in Far East Asian countries, such as South Korea and Japan. Particularly in South Korea, it takes the lead as the primary cultured marine fish, reaching a production of 46,000 tons in 2022, constituting 50.5% of the total aquaculture production in the country[4]. Meanwhile, other countries, like the United States, are also recognizing the olive flounder as a promising candidate for aquaculture due to its high market value and advantageous traits for domestic cultivation. In fact, *P. olivaceus*exhibits an exceptional food conversion ratio compared to other flatfish species, and therefore requires a relatively short period of time for growth[5].

However, olive flounder cultivation often encounters issues that significantly impact its yields, with one of the major reasons being infectious diseases caused by various microbial agents, including bacteria, viruses, and parasites[6–8]. Among these, *Vibrio scophthalmi* has been identified as an opportunistic bacterial pathogen, being the most prevalent within the intestines of diseased olive flounder and turbot[9–11]. Indeed, when olive flounder is subjected to environmental stress, compromising its immunity, the presence of *V. scophthalmi*increases the fish's vulnerability[12,13]. Similarly, multispecies infection by *V. scophthalmi* and another fish pathogen, *Streptococcus parauberis*, significantly raises the mortality rate of the fish compared to infections with either species alone[13].

Bacterial pathogens often communicate with each other to synchronize their gene expressions for group behaviors, such as the production of virulence factors[14–16]. This phenomenon, known as quorum sensing (QS), involves the bacterial production and release of small molecules called autoinducers (AIs), which enable bacteria to detect their population density[17,18]. In *Vibrio harveyi* and *Vibrio cholerae*, for example, multiple AIs are synthesized and detected by distinct transmembrane receptor proteins. At low cell density (LCD), these transmembrane receptors undergo autophosphorylation, transferring a phosphate group to the common response regulator, LuxO, via the phospho-relay protein LuxU. Subsequently, phospho-LuxO, together with σ-54, activates the transcription of small regulatory RNAs, which in turn down-regulates the expression of the quorum sensing master regulator, LuxR. At high cell density (HCD), AI binding to the receptors reverses the phosphate flow in the cell, leading to the translational production of LuxR proteins[19–21]. It is noteworthy that LuxR homologues are often referred to by various names in different species, such as $LuxR_{Vh}$ in *V. harveyi*, HapR in *V. cholerae*, and SmcR in *V. vulnificus*[22–24].

Previous studies have suggested that *V. scophthalmi*produces two AIs and possesses a QS system similar to that of other vibrios[25,26]. Indeed, a LuxR homologue in *V. scophthalmi* (hereafter referred to as $LuxR_{Vs}$) exhibits 81.86% identity with *V. vulnificus*SmcR at amino acid sequence level[26,27]. Biofilm formation has been proposed as a QS-regulated phenotype in *V. scophthalmi*, but scarcely genetic or molecular basis has been indicated[26]. In addition, although QS regulon have been explored in some clinically relevant *Vibrio*species[28–31], no genome-wide analysis exploring LuxR-mediated QS regulon has been conducted for this important fish pathogen. Consequently, it remains ambiguous how diverse genes and physiologies are under the control of QS in *V. scophthalmi*, which significantly affecting olive flounder production.

To address this gap, here we analyzed the chromosome of the *V. scophthalmi* 21FBVib0096, isolated from a diseased olive flounder. Subsequently, we conducted a genome-wide transcriptomic analysis comparing the wild-type and the $luxR_{Vs}$ deletion mutant ($\Delta luxR_{Vs}$). Through these analyses, we successfully identified numerous $LuxR_{Vs}$ regulon. By employing the gene ontology (GO) and Kyoto Encyclopedia of Genes and Genomes (KEGG) pathway enrichment analyses, we further gained valuable insights into the functional implications of $LuxR_{Vs}$-mediated QS in *V. scophthalmi*. The results represent an initial step toward a deeper understanding of the pathogen's physiology, which could be modulated to reduce its pathophysiological traits and thus improve seafood production.

Results

Genomic information of *V. scophthalmi* 21FBVib0096

The genome of *V. scophthalmi* 21FBVib0096, isolated from a diseased *P. olivaceus* by the National Institute of Fisheries Science in 2021, was sequenced and analyzed following the procedures summarized in the Materials and Methods section. The genome consisted of two circular chromosomes [chromosome I (3,352,351 bp, GC content 44.95%) and chromosome II (1,419,321 bp, GC content 44.01%)], along with one plasmid (100,413 bp, GC content 44.13%) (Fig. 1). In chromosome I, a total of 3,193 genes were identified, including 3,060 coding sequences (CDSs), 95 tRNA genes, 37 rRNA genes, and 1 tmRNA. Chromosome II contained 1,300 genes with 1,290 CDSs and 10 tRNA genes. The plasmid comprised 124 genes with 123 CDSs and 1 tRNA gene. Overall, out of 4,473 CDSs in the whole genome, 2,807 (62.75%) were annotated as functional genes, while the remaining, 1,666 CDSs (37.25%) were categorized as hypothetical or uncharacterized proteins. Gene annotation of *V. scophthalmi* 21FBVib0096 revealed the presence of multiple QS components, including LuxU and LuxO, indicating that the pathogen likely possesses a functional QS system (Supplementary Table S1). Among, *Vs096_03041*, a gene encoding QS master regulator $LuxR_{Vs}$, is in the chromosome I. Accordingly, this gene was targeted for deletion mutation, and the resulting $\Delta luxR_{Vs}$ strain was used for subsequent transcriptomic analyses.

Identification of $LuxR_{Vs}$ regulon via RNA-sequencing

To identify $LuxR_{Vs}$ regulon, we compared the whole transcriptomes of $\Delta luxR_{Vs}$ and wild-type *V. scophthalmi* under HCD condition (MT-HCD vs. WT-HCD; in the Supplementary Figure S1) via RNA-sequencing. In the

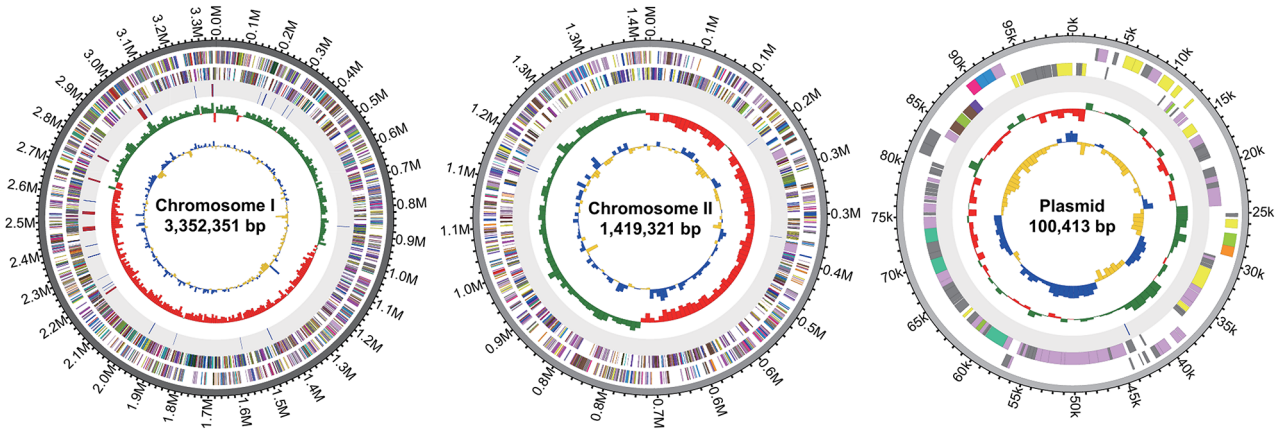


Fig. 1. Genome of ***V. scophthalmi*** 21FBVib0096. Two chromosomes and one plasmid are shown. The outermost circle indicates positions in megabase (for chromosomes) or kilobase (for plasmid) scale. The second circle illustrates coding sequences on both the forward and reverse strands. The third circle denotes tRNA (blue) and rRNA (red) positions. The fourth circle displays GC-skew [(G-C)/(G + C)], with green and red bands denoting positive and negative values, respectively. The fifth circle represents the GC-content, where blue and yellow bands indicate values above or below 50%, respectively.

meantime, we also compared the transcriptomes of the wild-type strain under both LCD and HCD conditions (WT-LCD vs. WT-HCD; Supplementary Fig. S1) to evaluate the influence of growth status on gene expression patterns. Each sample was prepared in triplicate, generating an RNA-sequencing dataset comprising a total of 549,231,520 reads, of which 436,286,522 reads successfully mapped to the *V. scophthalmi* genome. Quality assessment indicated high Q20 and Q30 percentages, surpassing 98% and 94%, respectively (Supplementary Table S2). Notably, the gene expression profiles of all three samples in each condition, except for MT-HCD3, exhibited a similar pattern in both multidimensional scaling (Supplementary Fig. S2a) and hierarchical clustering analyses (Supplementary Fig. S2b). Consequently, a total 8 transcriptome profiles (MT-HCD1 and 2; WT-HCD1-3; and WT-LCD1-3) were used in further analyses.

In the comparison of MT-HCD vs. WT-HCD, 631 differentially expressed genes (DEGs; |fold change| $\geq$ 1.75 and $p \leq 0.05$) were identified, comprising 366 up-regulated and 265 down-regulated genes in the MT-HCD compared to the WT-HCD (Fig. 2a, Supplementary Fig. S3a, and Supplementary Dataset S1). In the comparison of WT-LCD vs. WT-HCD, a total of 2,121 genes exhibited differential expression, with 1,024 up-regulated and 1,097 down-regulated genes in the WT-LCD compared to the WT-HCD (Fig. 2a, Supplementary Fig. S3b, and Supplementary Dataset S2). Further comparative analysis of the two comparisons revealed a set of 332 overlapping DEGs. Among these, 94 genes exhibited an up-regulated pattern in both comparisons, while 115 genes exhibited a down-regulated pattern in both comparisons (Fig. 2b). In the meantime, the remaining 123 genes showed a contrasting expression pattern in the two comparisons, where 85 genes exhibited an up-regulated pattern in the MT-HCD vs. WT-HCD but a down-regulated pattern in the WT-LCD vs. WT-HCD, and 38 genes exhibited vice versa (Fig. 2b). The list of overlapping DEGs for each category is provided in Supplementary Dataset S3.

To further validate the differential gene expression patterns observed, thirteen genes representing the aforementioned categories were selected for quantitative Real-Time PCR (qRT-PCR) analysis. Specifically, *bccT3* and *Vs096_04402* were selected from the $LuxR_{Vs}$ regulon, while *cysK* and *hutU* were chosen to represent growth status-dependent genes. From the overlapping DEGs, *Vs096_01435*, *guaB*, and *Vs096_03709* were selected as coincidentally up-regulated genes, while *degP*, *phaC*, and *phaB* were selected as coincidentally down-regulated genes. For the contrastingly regulated DEGs, *Vs096_00748*, *vpsT*, and *Vs096_04425* were chosen. As shown in Fig. 2c and d, the qRT-PCR results were highly consistent with the RNA-sequencing data, further confirming the reliability of our whole transcriptome sequencing analysis.

Overall, the transcriptome analyses revealed the $LuxR_{Vs}$ regulon, comprising 631 genes, of which 332 are co-regulated by the cell growth status, whereas 299 are part of the growth independent $LuxR_{Vs}$ regulon.

Functional profiling of $LuxR_{Vs}$ regulon

To elucidate the regulatory role of $LuxR_{Vs}$ and how cell growth status affects $LuxR_{Vs}$-mediated physiologies, we functionally classified the identified DEGs through GO and KEGG pathway analyses. The GO enrichment analysis for DEGs from the MT-HCD vs. WT-HCD comparison revealed up-regulation of osmoprotection-related molecular process and membrane transporter activities in the MT-HCD. These included glycine betaine transport, dicarboxylic acid transport, symporter activity, carbohydrate transport, and carbohydrate transmembrane transporter activity (Fig. 3a). Notably, diguanylate cyclase activity was also significantly enriched as an up-regulated GO term in the MT-HCD compared to the WT-HCD (Fig. 3a), suggesting a suppression of cyclic bis-(3', 5')-dimeric guanosine monophosphate (c-di-GMP) biosynthesis by $LuxR_{Vs}$ in *V. scophthalmi* at HCD. In a meantime, the MT-HCD also exhibited significant enrichment of down-regulated biological processes and molecular functions compared to the WT-HCD. These down-regulated processes included unfolded protein

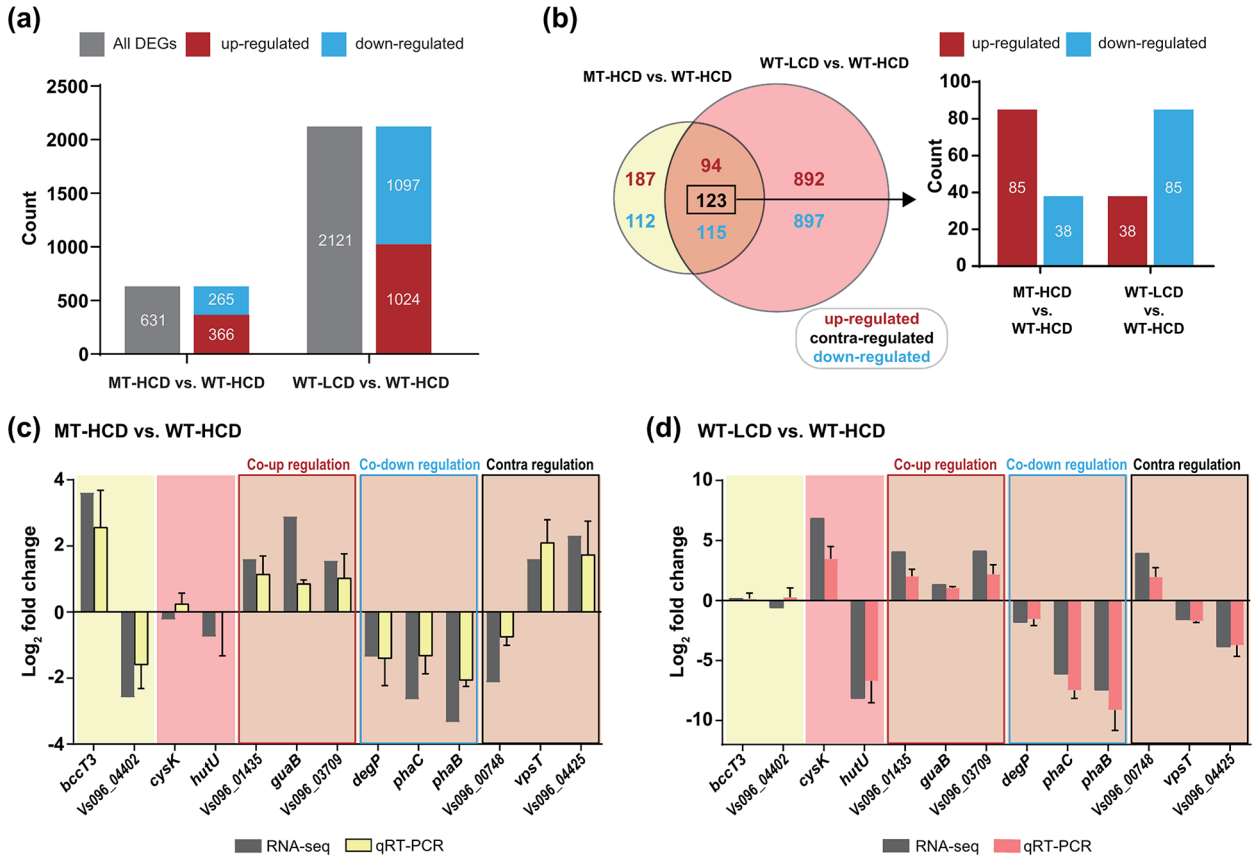


Fig. 2. Overview of differentially expressed genes (DEGs) identified by RNA-sequencing. **(a)** The total number of DEGs (gray), as well as up-regulated (red) and down-regulated (blue) DEGs revealed in the MT-HCD vs. WT-HCD comparison and the WT-LCD vs. WT-HCD comparison, are shown. **(b)** A Venn diagram illustrating the number of DEGs from both comparisons is shown. The overlapping DEGs were further categorized into coincidentally up- or down-regulated DEGs and contrastingly regulated DEGs, with their respective numbers depicted as bar graphs. **(c and d)** Validation of RNA-sequencing data via qRT-PCR analysis. The fold changes in expression of the indicated genes in either the MT-HCD (**c**) or WT-LCD (**d**) sample are presented relative to those in the WT-HCD sample. The *recA* gene was used as internal reference for qRT-PCR.

binding, iron ion transport, oxidoreductase activity, and metabolic processes for tricarboxylic acids, dicarboxylic acids, and carbohydrate derivatives (Fig. 3b).

GO enrichment analysis for DEGs from the WT-LCD vs. WT-HCD comparison revealed the up-regulation of ribosome-related GO terms (Fig. 3c). These terms included cytosolic small/large ribosomal subunits and structural constituent of ribosome, suggesting relatively increased translational activity in early exponential phase cells (WT-LCD) compared to stationary phase cells (WT-HCD). Conversely, diverse GO terms, such as tricarboxylic acid cycle, oxidoreductase complex, respiratory electron transport chain, and peptide transport were down-regulated in the WT-LCD compared to the WT-HCD (Fig. 3d).

Consistent with the GO analysis results, the KEGG pathway analysis identified relevant pathways. In the comparison of MT-HCD vs. WT-HCD, KEGG analysis revealed significant enrichment in a total of 140 pathways from 222 DEGs. Among these, the up-regulated genes in the MT-HCD compared to the WT-HCD significantly clustered into pathways involved in nitrogen metabolism, phosphotransferase system, ABC transporters, and biofilm formation (Fig. 4a). Conversely, the down-regulated genes in the MT-HCD compared to the WT-HCD were associated with pathways responsible for amino acid and carbohydrate metabolism (Fig. 4b).

In the comparison between WT-LCD and WT-HCD, 883 DEGs were classified into 230 pathways. Significantly up-regulated pathways in the WT-LCD compared to the WT-HCD included ribosome and purine metabolism (Fig. 4c), while significantly down-regulated pathways encompassed the two-component system, quorum sensing, glyoxylate/dicarboxylate metabolism, and the citrate cycle (Fig. 4d). Notably, the pyruvate metabolism and butanoate metabolism pathways were identified as significantly down-regulated in both MT-HCD vs. WT-HCD (Fig. 4b) and WT-LCD vs. WT-HCD (Fig. 4d) comparisons.

LuxR$_{Vs}$-mediated up-regulation of poly-hydroxyalkanoate (PHA) biosynthesis

Because the KEGG pathway enrichment analysis revealed significant down-regulation of butanoate metabolism in both comparisons (Fig. 4b and d), we further inspected the DEGs associated with this pathway. The butanoate

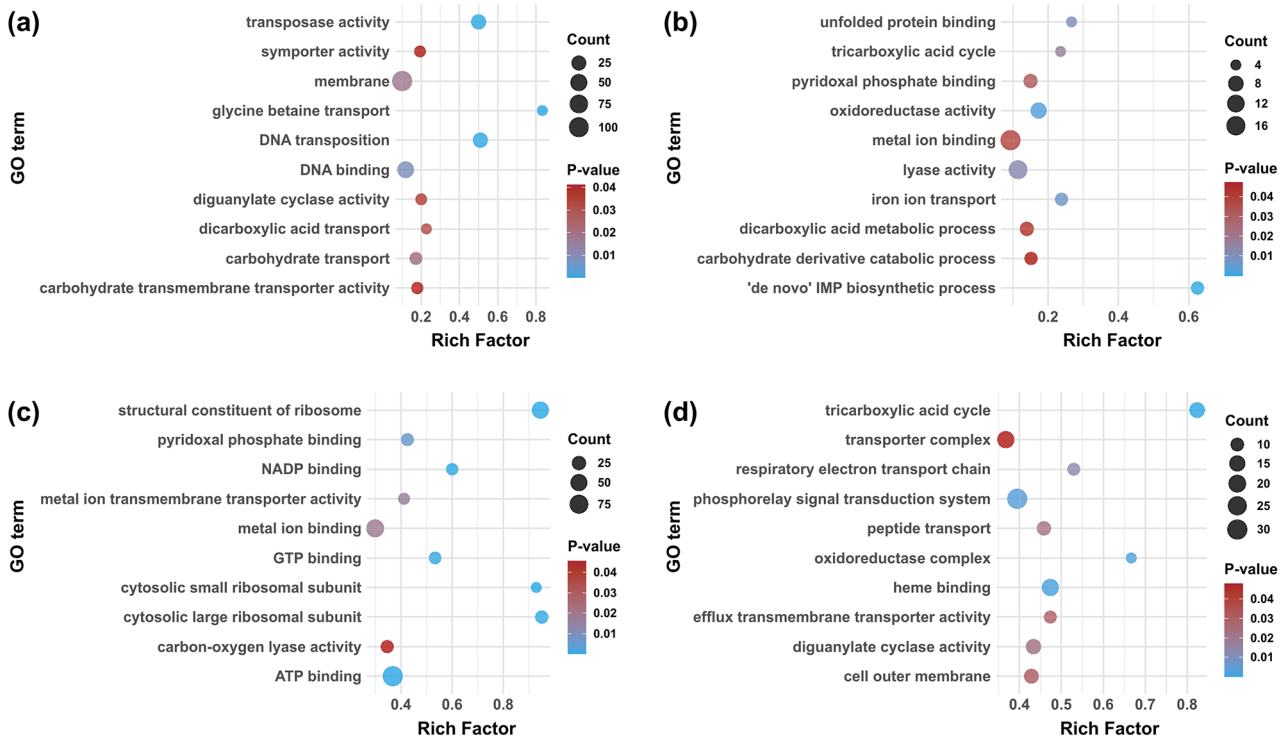


Fig. 3. GO enrichment analysis for DEGs. Up-regulated (**a** and **c**) and down-regulated (**b** and **d**) DEGs from the comparisons of MT-HCD vs. WT-HCD (**a** and **b**) and WT-LCD vs. WT-HCD (**c** and **d**) were analyzed by GO enrichment. On the y-axis, GO terms are represented, while the x-axis shows the corresponding rich factor of each term. The color intensity and size of the points correspond to the *p*-value and the number of DEGs associated with each GO term, respectively.

metabolism is known to be interconnected with the citrate cycle (TCA cycle), glycolysis, and the metabolic pathways of amino acids and fatty acids[32,33]. Consistent with this, genes encoding citrate cycle enzymes (e.g., fumarate reductase, Vs096_02777-80; succinate dehydrogenase, Vs096_01705-08 and Vs096_03353) and those involved in amino acid-related metabolic pathways (e.g., acetolactate synthase, Vs096_02022-23 and Vs096_02587) were significantly down-regulated in the MT-HCD and/or WT-LCD compared to the WT-HCD (Fig. 5a and Supplementary Datasets S1 and S2).

Notably, the expression of PHA synthase gene and related genes, including acetyl-CoA acetyltransferase (Vs096_03255, *phaA*), acetoacetyl-CoA reductase (Vs096_03256, *phaB*), PHA synthase (Vs096_03253, *phaC*), and phasin (Vs096_03254, *phaP*), was also markedly suppressed in both MT-HCD and WT-LCD samples compared to the WT-HCD (Fig. 5a). Indeed, the fold change values of the *phaBAPC* genes in the MT-HCD were −10.12, −9.00, −10.25, and −6.30, and those in the WT-LCD were −176.76, −156.99, −235.23, and −70.29, when compared to the WT-HCD (Fig. 5b). These findings suggest that $LuxR_{Vs}$ and growth status mediate the regulation of PHA biosynthesis.

To further investigate the role of $LuxR_{Vs}$ in PHA synthesis, we compared PHA levels in the wild-type, Δ$luxR_{Vs}$, and complemented strains. As shown in Fig. 5c, the wild-type and complemented strains, but not the Δ$luxR_{Vs}$ strain, exhibited intense pink fluorescent colonies on the Nile red containing plate under UV light, indicating substantial accumulation of PHA in the cells. Consistent with this result, quantitative analysis via Nile red fluorescence method confirmed that the Δ$luxR_{Vs}$ strain had the lowest PHA production level. Notably, complementation with the $luxR_{Vs}$ gene significantly enhanced PHA production over the wild-type level (Fig. 5d), likely due to the effects of multicopy complementation. When the *smcR* gene, a *luxR* homologous gene in *V. vulnificus*, was used instead of the $luxR_{Vs}$ gene, restoration of PHA level was also achieved, albeit with less PHA level than the $luxR_{Vs}$ complementation (Fig. 5c and d). Collectively, these findings demonstrate that $LuxR_{Vs}$ plays a positive role in enhancing PHA biosynthesis by activating genes involved in butanoate metabolism and PHA synthesis, and that $LuxR_{Vs}$ and SmcR are functional homologs of each other.

$LuxR_{Vs}$-mediated down-regulation of biofilm formation

Because diguanylate cyclase activity and biofilm formation were significantly enriched in the GO term and KEGG pathway analyses, respectively (Figs. 3a and 4a), we also inspected the DEGs related to c-di-GMP synthesis and biofilm formation. In *V. cholerae*, a well-known *Vibrio* species recognized for its biofilm formation, a polar flagellum and mannose-sensitive hemagglutinin (MSHA) pili aid cells in scanning and attaching to surfaces, and the VPS (*Vibrio*polysaccharide) extracellular matrix is utilized in biofilm formation. During this process, c-di-GMP, synthesized by diguanylate cyclase, plays a critical role by binding to the key transcriptional

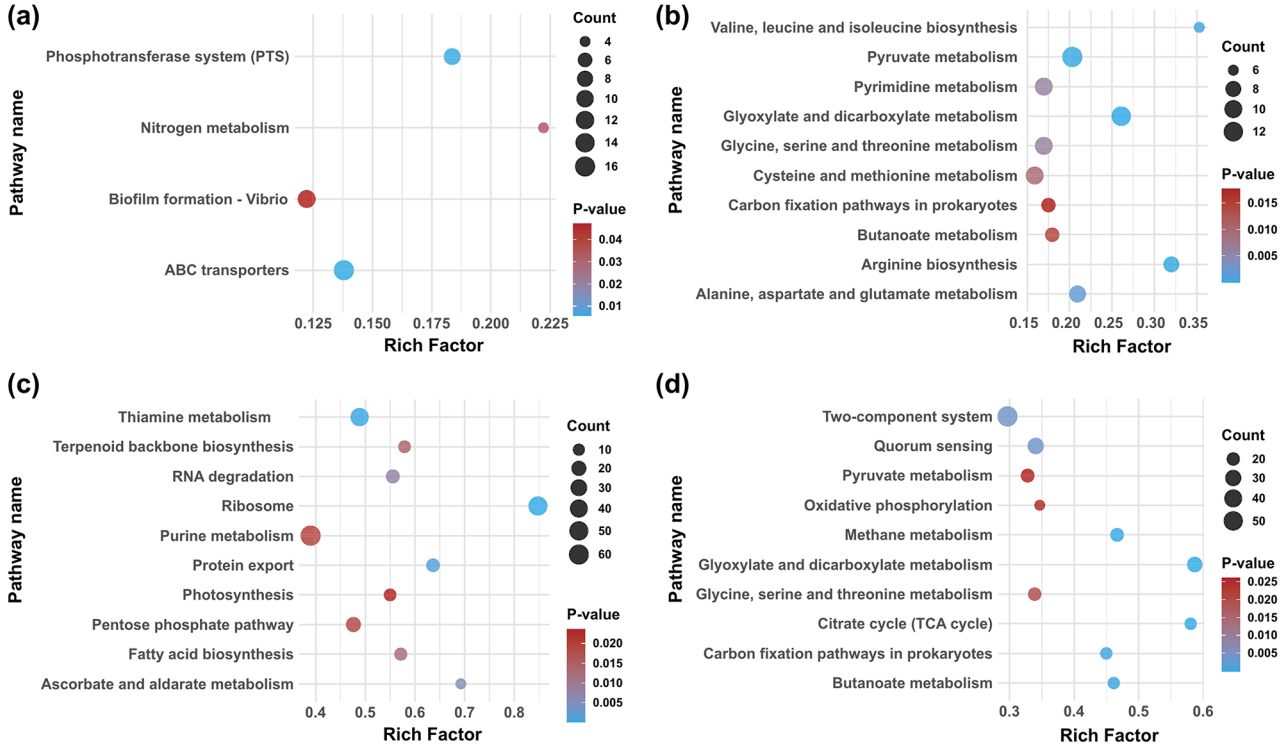


Fig. 4. KEGG pathway enrichment analysis for DEGs. Up-regulated (**a** and **c**) and down-regulated (**b** and **d**) DEGs from the comparisons of MT-HCD vs. WT-HCD (**a** and **b**) and WT-LCD vs. WT-HCD (**c** and **d**) were analyzed by KEGG pathway enrichment. On the y-axis, the pathway names are represented, while the x-axis shows the corresponding rich factor of each pathway. The color intensity and size of the points correspond to the p-value and the number of DEGs associated with each pathway, respectively.

regulator, VpsT, which in turn activates the *vps*operons and other biofilm-related genes[16]. Consistent with these previous reports, we found that the MSHA pilus gene *mshC* (Vs096_00555) and the diguanylate cyclase gene *cdgA* (Vs096_03429) in *V. scophthalmi* were significantly up-regulated in the MT-HCD (2.02-fold change for both genes) and WT-LCD (1.76- and 2.03-fold changes, respectively) compared to the WT-HCD (Fig. 6a and b). Notably, the expression of genes involved in the VPS production (e.g., glycosyltransferase *vpsL*, Vs096_03444; VPS biosynthesis/export protein *vpsN*, Vs096_03443; VPS-related tyrosine kinase *vpsO*, Vs096_3442; and VPS biosynthesis protein *vpsQ*, Vs096_03539) and the transcription activation for *vps* operons (i.e., transcriptional regulator *vpsT*, Vs096_03818) were significantly enhanced in the MT-HCD compared to the WT-HCD (Fig. 6a). Indeed, the fold change values of these genes in the MT-HCD were 2.93, 4.59, 3.86, 1.93, and 3.05, when compared to the WT-HCD (Fig. 6b). These findings suggest that $LuxR_{Vs}$ suppresses the VPS production and biofilm formation at HCD.

To validate this finding, we compared the biofilm formation activity of the wild-type, $\Delta luxR_{Vs}$, and complemented strains. As shown in Fig. 6c, the biofilm biomass of the $\Delta luxR_{Vs}$ strain was 1.45-fold higher than that of the wild-type strain. When this mutant strain was complemented with the $luxR_{Vs}$ gene, biofilm formation was reduced to an even slightly lower level than that of wild-type strain. As similar to the PHA production (Fig. 5c and d), the complementation with *smcR* gene also reverted the phenotype but to a lesser extent than that with the $luxR_{Vs}$ gene (Fig. 6c). Altogether, the results demonstrate that $LuxR_{Vs}$ negatively regulates the biofilm formation in *V. scopthalmi* by repressing the expression of MSHA pili MshC, diguanylate cyclase CdgA, and series of VPS biosynthesis genes.

Discussion

Because the QS system plays a role in regulating various bacterial physiologies, including virulence factor expression[14,15], we employed transcriptome analysis in this study to elucidate the global regulatory network controlled by $LuxR_{Vs}$, the QS master regulator in *V. scophthalmi*. In the comparison of $\Delta luxR_{Vs}$ and wild-type strains (i.e. MT-HCD vs. WT-HCD), we found that $LuxR_{Vs}$ significantly influences approximately 13.7% of the *V. scophthalmi* genome (631 genes out of a total of 4,617 genes; Fig. 2a). While this is considerably less than the number of genes regulated by growth status (as revealed in the comparison of WT-LCD and WT-HCD, 45.9%; 2,121 genes out of a total of 4,617 genes; Fig. 2a), this result confirms that $LuxR_{Vs}$ acts as a global transcriptional regulator in this fish pathogen, similar to other clinically relevant *Vibrio*species[28,29].

Among the total of 631 $LuxR_{Vs}$ regulon, more than 52.6% (332 genes) were also identified as DEGs controlled by the growth status (i.e. from the WT-LCD vs. WT-HCD comparison; Fig. 2b). Additional analysis further categorized this subset into four different groups based on their co-regulation and contrasting regulation

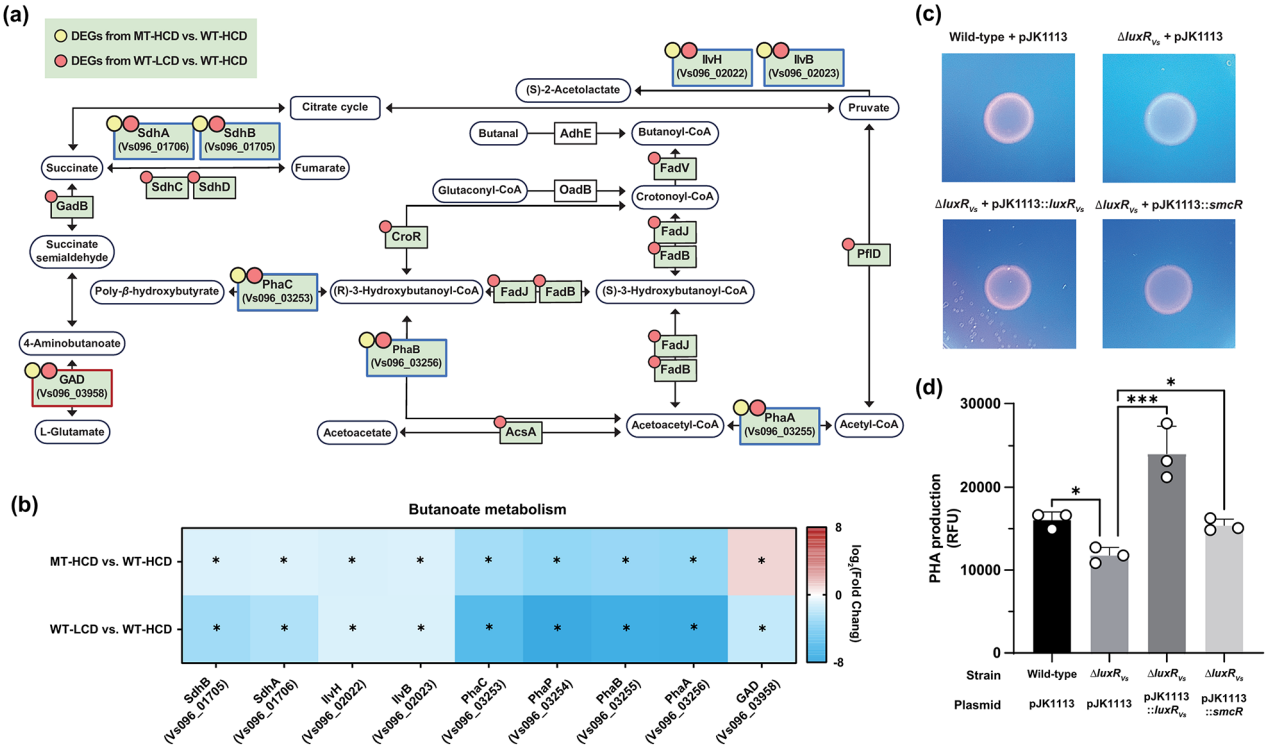


Fig. 5. LuxR$_{Vs}$enhances butanoate metabolism pathway and PHA production. **(a)** Schematic representation of the butanoate metabolism pathway with integrated PHA biosynthesis. Enzymes enriched in the KEGG pathway analysis are indicated with green boxes. Within these boxes, DEGs from the MT-HCD vs. WT-HCD and the WT-LCD vs. WT-HCD comparisons are annotated with yellow and pink dots, respectively, at the top-left corner. Among the overlapping DEGs from both comparisons, coincidentally down-regulated DEGs are indicated with blue frames. (Copyright Kanehisa laboratories; reproduced with permission[55].) **(b)** A heat map illustrating the $\log_2$ fold changes in the expression of key genes related to butanoate metabolism and PHA biosynthesis is presented for the MT-HCD vs. WT-HCD and the WT-LCD vs. WT-HCD comparisons. An asterisk (*) represents a statistically significant change in gene expression (|fold change| ≥ 1.75 and $p \leq 0.05$). **(c and d)** PHA production in the wild-type, Δ*luxR*$_{Vs}$, and complemented strains were examined by Nile red plate assay (**c**) and fluorescence method (**d**). Normalized PHA production levels are presented as means ± standard deviation (SD) from three independent experiments. Statistical significance was assessed by one-way ANOVA with Tukey's multiple comparisons (***, $p < 0.005$; *, $p < 0.05$).

patterns in two comparisons. First, 94 genes were up-regulated in both MT-HCD and WT-LCD experimental samples than the WT-HCD control sample, indicating that they are repressed at HCD with the help of LuxR$_{Vs}$ (Fig. 2b). In contrast, the second group, comprising 115 co-downregulated genes, displays reduced expression in both experimental samples compared to the WT-HCD control, suggesting that they are highly expressed at HCD with the help of LuxR$_{Vs}$-mediated activation (Fig. 2b). Considering that *Vibrio*LuxR homologues are highly translated only at HCD[17,18], these co-regulations may represent a *V. scophthalmi*'s effective strategy to reinforce the cell density-dependent regulation of genes by incorporating the LuxR$_{Vs}$-mediated regulation. For instance, the *aphA*gene (Vs096_02787), which encodes the LCD-specific QS master regulator[18,21], is repressed at HCD and by LuxR$_{Vs}$. In contrast, the *luxS* gene (Vs096_02054), encoding the AI-2 synthase, is activated at HCD and by LuxR$_{Vs}$ (Supplementary Dataset S1 and Supplementary Fig. S3). These reinforced regulations of QS components prevent *V. scophthalmi* from dysregulating the QS regulon, which could otherwise be affected by unintended AphA-mediated regulation and/or insufficient AI-2 production even at HCD.

Third and fourth groups, containing 85 and 38 genes respectively, exhibited contrasting expression patterns in the two comparisons (i.e. MT-HCD vs. WT-HCD and WT-LCD vs. WT-HCD; Fig. 2b). In general, genes in microbes are regulated in response to various environmental cues, including changes in cell density, and this allows them to cope effectively with various challenges, ensuring their survival. Therefore, the observed contrasting regulations in third and fourth groups may represent another intelligent strategy employed by *V. scophthalmi* to precisely regulate important subsets of LuxR$_{Vs}$ regulon, not simply through growth phase-dependent metabolic and/or environmental changes, but more specifically via QS-mediated bacterial communication.

Our study also revealed that *V. scophthalmi* activates genes in the biosynthetic pathway for PHA production through the LuxR$_{Vs}$ (Figs. 2c and 5). PHA is a bacterial intracellular semi-crystalline polymer that bacteria synthesize and store as granules when they encounter nutrient limitations or stress[37]. Therefore, our finding suggests that *V. scophthalmi* would experience nutrient starvation when crowded in a certain local environment, such as biofilms, and thus had evolved the QS-dependent PHA production mechanism. Alternatively, PHA

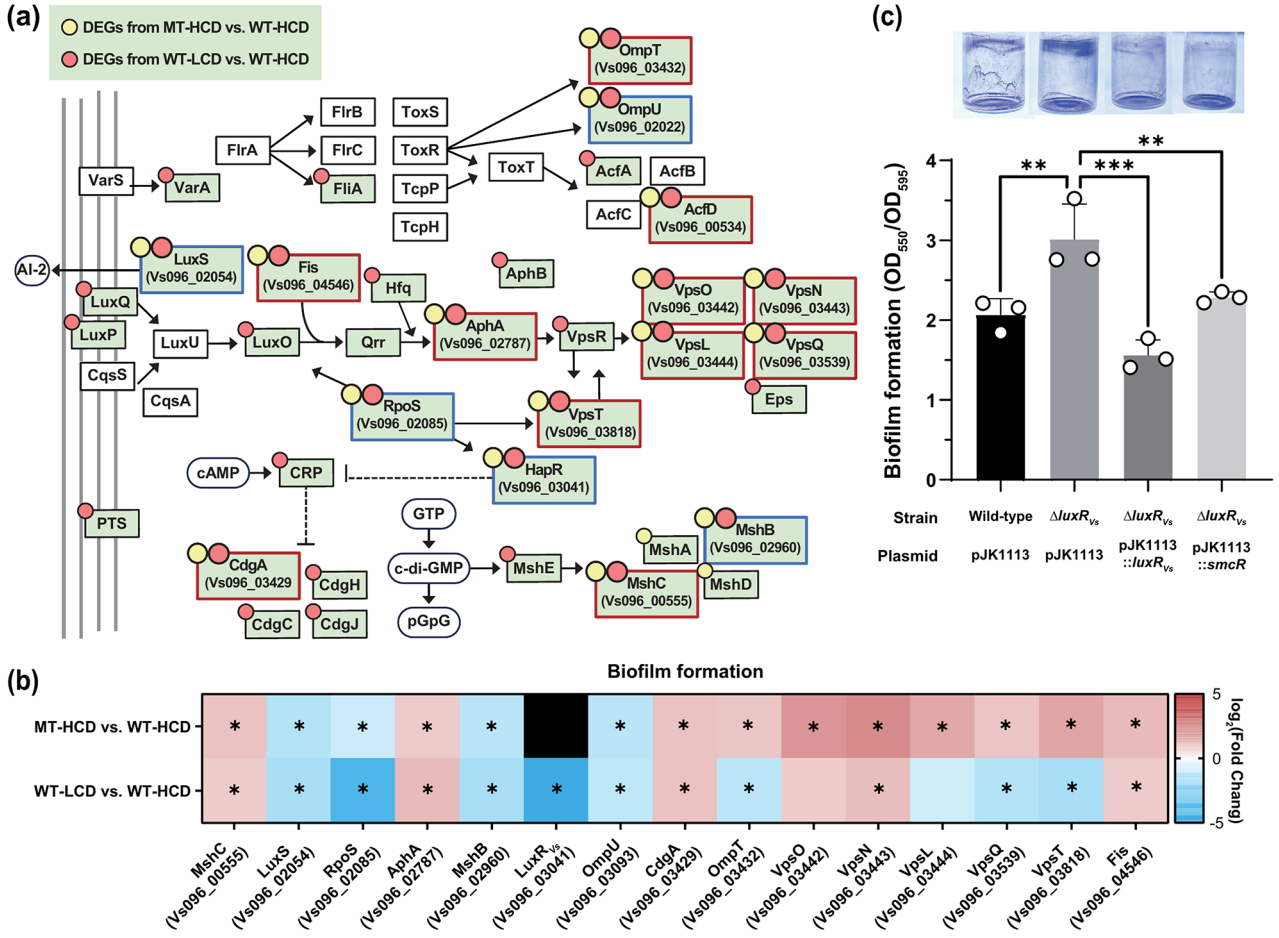


Fig. 6. LuxR$_{Vs}$negatively regulates biofilm formation. **(a)** Schematic representation of the biofilm formation pathway in vibrios. Proteins enriched in the KEGG pathway analysis are indicated with green boxes, in which the DEGs from the MT-HCD vs. WT-HCD and the WT-LCD vs. WT-HCD comparisons are marked with yellow and pink dots, respectively. Among the overlapping DEGs from both comparisons, up- or down-regulated DEGs from the MT-HCD vs. WT-HCD comparison are indicated with red or blue frames, respectively. (Copyright Kanehisa laboratories; reproduced with permission[55].) **(b)** A heat map illustrating the $\log_2$ fold changes in the expression of key biofilm formation pathway genes is presented for the MT-HCD vs. WT-HCD and the WT-LCD vs. WT-HCD comparisons. An asterisk (*) represents a statistically significant change in gene expression (|fold change| $\geq$ 1.75 and $p \leq 0.05$). Since the *luxR*$_{Vs}$ gene is deleted in the mutant, the corresponding part is left as black. **(c)** Biofilm formation of the wild-type, Δ*luxR*$_{Vs}$, and complemented strains in borosilicate tube was assessed by crystal violet staining. The stained tubes were photographed before the dye elution with ethanol (upper image). In the lower bar graph, normalized biofilm formation levels are presented as means ± SD from three independent experiments. Statistical significance was assessed by one-way ANOVA with Tukey's multiple comparisons (***, $p < 0.005$; **, $p < 0.01$).

biosynthesis at HCD might serve as a survival strategy for *V. scophthalmi*as it sheds from the fish host into the sea during its pathogenesis cycle. Indeed, this fish pathogen would proliferate high in the diseased host's intestine but is ultimately released into the nutrient-limited marine environment to initiate the next infection cycle[34–36]. In this context, the pathogen likely evolved to synthesize PHA granules within the crowded niche (i.e. the host intestine) to prepare and ensure survival upon encountering the open marine environment. In fact, several other bacterial species, including *Pseudomonas chlororaphis*, *Burkholderia thailandensis*, and *V. harveyi*, have also been reported to regulate PHA biosynthesis via QS, although their specific QS systems and components differ from each other and those in *V. scophtalmi*[37,38]. While details about *V. scophtalmi* pathogenesis remain to be elucidated, our findings, along with previous reports, contribute to a more comprehensive understanding of the bacterial survival strategies in marine environments by suggesting the role of QS in nutrient reservation.

In the meantime, PHA is also considered as a sustainable alternative to petroleum-based plastics because of its biodegradability. In fact, a few *Vibrio*species have been explored as potential candidates for PHA production, albeit the studies simply overexpressed the PHA biosynthesis genes or operon[39,40]. Since the PHA biosynthetic pathway is intrinsically linked to the butanoate metabolism pathway (Fig. 5a), metabolic engineering targeting the entire butanoate metabolism pathway could warrant higher production of PHA or PHA derivatives. In this aspect, our finding that the QS system activates many parts of the butanoate pathway via LuxR$_{Vs}$-mediated

regulation in *V. scophthalmi* (Fig. 5a) provides an important foundation for future engineering of this or related *Vibrio* species as a next-generation host for PHA fermentation.

Another key finding in this study is that the *V. scophthalmi* QS system negatively regulates biofilm formation via $LuxR_{Vs}$-mediated regulation of various biofilm-related genes (Fig. 6). In fact, a previous study reported exactly contradictory results, showing that deletion of the *luxR* or *luxS* gene in the *V. scophthalmi*A102 strain resulted in reduced biofilm formation[26]. The strain and medium (marine broth) used in the previous study differ from those in our study, which might explain the opposing results. Nonetheless, our transcriptome analysis, qRT-PCR validation, and phenotypic comparison, including the complemented strains (Figs. 2c and 6), clearly demonstrate that *V. scophthalmi* represses biofilm formation through the $LuxR_{Vs}$-mediated QS. Since c-di-GMP molecules governing biofilm formation are synthesized from two GTP molecules, the significant up-regulation of two genes in purine metabolism pathway [i.e., IMP dehydrogenase (Vs096_01797, *guaB*) and GMP synthase (Vs096_01798, *guaA*)] as well as the diguanylate cyclase gene (Vs096_03429, *cdgA*) in the $\Delta luxR_{Vs}$ strain compared to the wild-type strain (Figs. 2c and 6b, Supplementary Fig. S3a, and Supplementary Dataset S1) further supports our finding. Consistent with these, some other *Vibrio* species, such as *V. vulnificus* and *V. parahaemolyticus*, have also been reported to down-regulate biofilm formation through LuxR homologues[29,41].

Notably, genes related to osmoprotection were also found to be negatively regulated by $LuxR_{Vs}$ in *V. scophthalmi* (Fig. 3a). Indeed, biosynthesis genes for ectoine (Vs096_04335–04336, *ectAB*), one of the important compatible solutes in bacteria[42], were significantly up-regulated in the MT-HCD compared to the WT-HCD (Supplementary Dataset S1). Similarly, genes encoding betaine-carnitine-choline transporter 3 and ABC-family ProU transporter (Vs096_03282, *bccT3*; Vs096_04334 – 04332, *proVWX*), which are responsible for the uptake of compatible solutes[42], exhibited extreme up-regulation in the MT-HCD compared to the WT-HCD (Supplementary Fig. S3a and Supplementary Dataset S1). As suggested previously, this $LuxR_{Vs}$-mediated negative regulation of osmoprotection genes may represent a reduced necessity for compatible solutes in *V. scophthalmi*when this pathogen enters the HCD, a state for resting, not active adapting and replicating[43].

Importantly, we were unable to find any known toxins or type 3/4 secretion system apparatus in the *V. scophthalmi* genome (Fig. 1). Nonetheless, any enzymes that contribute to in vivo fitness, promoting the survival and proliferation of this opportunistic pathogen, could be potential virulence determinants. This is because fish possess various defense mechanisms against pathogen infection, including the production of reactive oxygen species (ROS) by macrophages. Consequently, invading pathogens must efficiently neutralize ROS to survive and proliferate in the face of host immune responses[44]. Consistently, a previous study has demonstrated that the activity of protective enzymes against host-derived ROS and free radicals is greater in hyper-virulent *V. scophthalmi*strains compared to less virulent strains[10]. Notably, genes encoding such enzymes, namely superoxide dismutase (Vs096_03760, *sod1*), alkyl hydroperoxide reductase subunit C (Vs096_02795, *ahpC*), and catalase (Vs096_03799, *katE*), were significantly down-regulated in the MT-HCD compared to the WT-HCD (Supplementary Fig. S3a and Supplementary Dataset S1), indicating $LuxR_{Vs}$-mediated activation. Since *V. scophthalmi* would proliferate to a much higher concentration within the host than in the open marine environment, the $LuxR_{Vs}$-mediated activation of such protective enzymes is not a simple cell-density dependent regulation but rather a form of spatiotemporal regulation. Therefore, it is clear that *V. scophthalmi* employs the QS system to precisely regulate these virulence traits, which are crucial for its survival and pathogenesis in the fish host.

In conclusion, this study provides critical insights into the global regulatory roles of the QS master regulator $LuxR_{Vs}$ in the fish pathogen *V. scophthalmi*. Our genomic and transcriptomic analyses reveal that $LuxR_{Vs}$ mediates the regulation of diverse physiological processes, including nutrient reservation (PHA biosynthesis), biofilm formation, osmoprotection, and virulence (Fig. 7). These functions are of particular relevance to the pathogen's ability to survive and proliferate in aquatic environments, where they significantly impact seafood production, as demonstrated in olive flounder cultivation. Importantly, the identification of $LuxR_{Vs}$ as a central global regulator highlights its potential as a target for mitigating the virulence of *V. scophthalmi* without compromising its viability (Supplementary Fig. S1), thus avoiding the risk of resistance development. The use of QS inhibitors, such as the previously characterized QStatin[29], presents a promising strategy for disrupting $LuxR_{Vs}$-mediated QS pathways, offering an innovative approach to managing bacterial infections in aquaculture. Given the growing concerns over microbial infections and antibiotic resistance in aquaculture worldwide[45], our findings offer a foundation for the development of more sustainable and effective measures to enhance seafood production.

Materials and methods

Bacterial strains and culture conditions

All bacterial strains and plasmids used in this study are listed in Table 1. Unless otherwise specified, *Escherichia coli* and *V. scophthalmi* strains were grown in Luria-Bertani medium (LB; BD Difco, Sparks, MD, USA) at 37 °C and in LB supplemented with 2.0% (w/v) NaCl (LBS) at 27 °C, respectively. Autoinducer bioassay (AB) medium (300 mM NaCl, 50 mM $MgSO_4$, 0.2% vitamin-free casamino acids, 10 mM potassium phosphate, 1 mM L-arginine, pH 7.5)[46]supplemented with 66.7 mM glycerol[47] was used for biofilm formation. When necessary, antibiotics were used at the following concentrations: for *E. coli*, 20 μg/ml chloramphenicol, 100 μg/ml ampicillin, and 100 μg/ml kanamycin; for *V. scophthalmi*, 3 μg/ml chloramphenicol, 100 μg/ml ampicillin, and 100 μg/ml kanamycin.

Whole genome sequencing, assembly, and annotation

Genomic DNA of the *V. scophthalmi* 21FBVib0096 strain was extracted using the G-spin™ Genomic DNA Extraction Kit (iNtRON Biotechnology, South Korea) and then sequenced using the MiSeq (Illumina Inc., San Diego, CA, USA) and the GridION (Oxford Nanopore Technologies, Oxford, UK) platforms at Sanigen Co. Ltd. (South Korea). Raw reads were subjected to *de novo*assembly using Unicycler (v0.4.8)[48]with circularization.

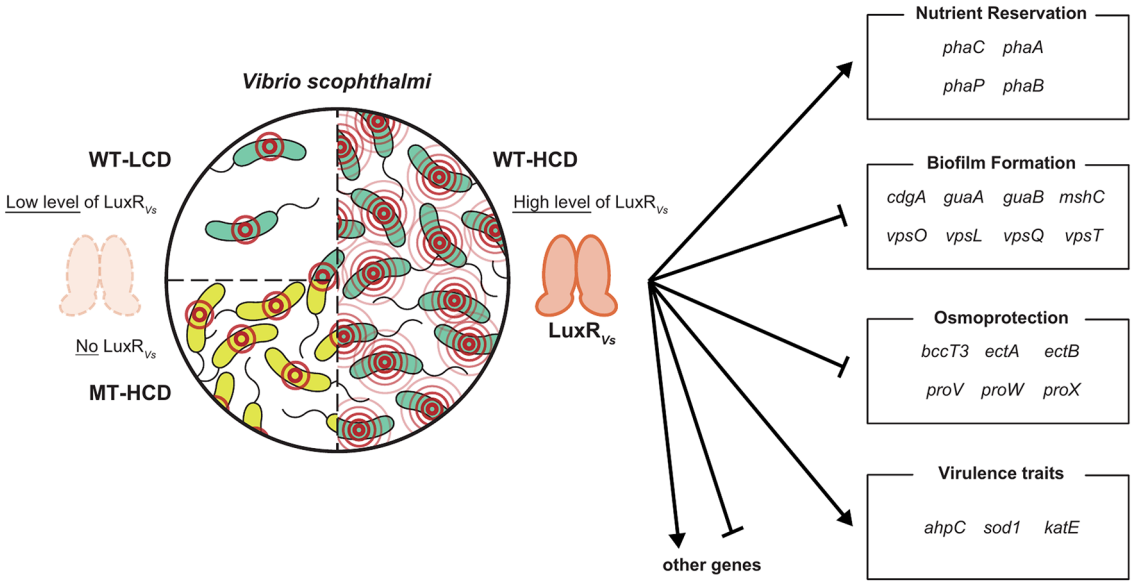


Fig. 7. LuxR$_{Vs}$-mediated regulation of group behaviors in ***V. scophtahlmi***. As cell density increases, LuxR$_{Vs}$ directly or indirectly regulates the expression of multiple downstream genes involved in various group behaviors. Nutrient reservation and virulence traits-related genes are positively regulated while biofilm formation and osmoprotection-related genes are negatively regulated by LuxR$_{Vs}$.

Bacterial strain or plasmid	Relevant characteristics [a]	Reference or source
Strains		
V. scophthalmi		
21FBVib0096	Wild-type; isolated from diseased fish	This study; NIFS [b]
21FBVib0096 Δ*luxR*$_{Vs}$	21FBVib0096 with Δ*luxR*$_{Vs}$	This study
E. coli		
DH5α	*supE44* Δ*lacU169* (*Φ80 lacZ* ΔM15) *hsdR17 recA1 endA1 gyrA96 thi-1 relAI*	Laboratory collection
S17-1 λ*pir*	λ*pir* lysogen; *thi pro hsdR hsdM*$^{+}$*recA* Tc::Mu-Km::Tn7;Tp^{r} Sm^{r}; host for π-requiring plasmids; conjugal donor	68
Plasmids		
pDS132	R6K γ*ori sacB*; suicide vector; *oriT* of RP4; Cm^{r}	69
pBK2301	pDS132 with Δ*luxR*$_{Vs}$; Cm^{r}	This study
pJK1113	pKS1101 with *nptI*; Ap^{r} Km^{r}	59
pBK2302	pJK1113 with *luxR*$_{Vs}$; Ap^{r} Km^{r}	This study
pBSS-WT	pBAD24 with *smcR*; Ap^{r}	27
pBK2303	pJK1113 with *smcR*; Ap^{r} Km^{r}	This study

Table 1. Bacterial strains and plasmids used in this study. [a] Tp^{r}, trimethoprim-resistant; Sm^{r}, streptomycin-resistant; Ap^{r}, ampicillin-resistant;. Cm^{r}, chloramphenicol-resistant; Km^{r}, kanamycin-resistant; Tc^{r}, tetracycline-resistant. [b] NIFS, National Institute of Fisheries Science, South Korea.

Annotation procedure was conducted at CJ Bioscience, Inc. (South Korea). Briefly, prediction of CDSs was carried out using PRODIGAL (v2.6.2)[49]. Transfer RNAs were identified using tRNAscan-SE (v1.3.1)[50]. Ribosomal RNAs and non-coding RNAs were predicted using covariance model search with Rfam 12.0 database[51]. Clustered regularly interspaced short palindromic repeats (CRISPRs) were identified using Piler-CR (v.1.06) program[52]and the CRISPR Recognition Tool (CRT) (v.1.2)[53]. Functional annotation was performed through homology search against databases, including EggNOG (v 4.1), KEGG, and SEED subsystems, utilizing the USEARCH program (v. 8.01517)[54–57]. The complete genome sequence of *V. scophthalmi* 21FBVib0096 strain has been deposited in the GenBank under accession numbers, CP134277 (chromosome 1), CP134278 (chromosome 2), and CP134279 (plasmid).

Construction of *luxR*$_{Vs}$ deletion mutant and complemented strains

Oligonucleotides used in this study are listed in the Supplementary Table S3. To construct an isogenic *luxR*$_{Vs}$ mutant, about 80% of the internal region of *luxR*$_{Vs}$ open reading frame was deleted in vitro employing the PCR-

mediated linker-scanning method. In brief, pairs of primers $LuxR_{Vs}$-F1 and -R1 or $LuxR_{Vs}$-F2 and -R2 were used for amplification of the 5' and 3' amplicons, respectively (Supplementary Table S3). The 481-bp-deleted $luxR_{Vs}$ gene was then amplified by PCR using a mixture of both amplicons as templates and primers $LuxR_{Vs}$-F1 and $LuxR_{Vs}$-R2. The resulting DNA fragment was treated with *Sph*I and *Sac*I and then ligated into the same enzyme-treated pDS132 to generate the pBK2301 (Table 1). Subsequently, the plasmid was transformed into *E. coli* S17-1 λ*pir* and then transferred into *V. scophthalmi*21FBVib0096 through conjugation. Exconjugants were isolated on selective plates (TCBS agar plates supplemented with chloramphenicol) and subjected to the sucrose challenge to facilitate the second homologous recombination, as previously described[58]. The desired mutation was verified by PCR and sequencing of the engineered $luxR_{Vs}$ gene region using primers $LuxR_{Vs}$-F and $LuxR_{Vs}$-R (Supplementary Table S3).

For complementation of the mutation, coding regions of the *V. scophthalmi* $luxR_{Vs}$ and *V. vulnificus smcR* were amplified from the *V. scophthalmi*21FBVib0096 genome and pBSS-WT vector[27], respectively, using specified primer sets (Supplementary Table S3). Each amplified product was cloned into *Nco*I-*Xba*I-digested pJK1113, an arabinose-inducible expression vector[59], resulting in the creation of pBK2302 and pBK2303, respectively (Table 1). The plasmids were then transferred into the *V. scophthalmi* Δ$luxR_{Vs}$ by conjugation as described above.

RNA isolation and transcriptome analysis

The wild-type and Δ$luxR_{Vs}$ strains were cultured in LBS at 27 °C for 9 h to ensure a HCD of the cultures, reaching stationary phase (Supplementary Fig. S1). Accordingly, the harvested samples from wild-type and mutant strains were designated as WT-HCD and MT-HCD, respectively. Total RNAs were isolated from the harvested samples using RNeasy Mini Kit (QIAGEN, Hilden, Germany) following the manufacturer's instructions. The RNA samples were then treated with DNase I to eliminate any genomic DNA and subsequently purified using RNeasy Minelute Cleanup Kit (QIAGEN). To prepare an LCD sample, wild-type cells grown to early exponential phase (Supplementary Fig. S1) were harvested, and their total RNA was purified. This sample was designated as WT-LCD.

RNA-sequencing was conducted as previously described[29] with slight modification at CJ Bioscience, Inc. Total RNA quantity and quality were assessed using ND-2000 spectrophotometer (Thermo Fisher Scientific, Madison, USA) and Agilent 2100 Bioanalyzer (Agilent Technologies, Santa Clara, CA, USA), respectively. Before the construction of strand-specific complementary DNA (cDNA) library, mRNA was firstly enriched by depleting ribosomal RNAs using NEBNext rRNA Depletion Kit (Bacteria) (New England BioLabs, Hitchin, UK). Libraries were prepared using the TruSeq® Stranded mRNA library prep kit (Illumina). Subsequently, sequencing was performed on the Illumina NovaSeq6000 platform using 150 bp paired-end sequencing. The raw sequencing reads were deposited in the NCBI Short Read Archive (SRA) under accession numbers SRR28019963 to SRR28019971. After preprocessing steps, including sequencing quality check and adapter trimming, the sequencing reads were mapped to the *V. scophthalmi*21FBVib0096 genome. By using the EdgeR package[60], raw read counts for each gene were normalized using the TMM algorithm to account for any systematic biases across the samples[61]. To elucidate expression patterns among sample groups, a multidimensional scaling (MDS) plot was created using the plotMDS function of EdgeR package[60]. Following this, hierarchical clustering was executed using the heatmap package with a squared Euclidean distance metric as the second analysis. Pairwise comparison analysis was then statistically performed to identify DEGs ($|\text{fold change}| \geq 1.75$ and $p \leq 0.05$) in the MT-HCD or WT-LCD sample relative to the WT-HCD sample.

For functional analysis of the DEGs, the transcriptome was aligned to the nonredundant (nr) database of the NCBI via blastx search with an E-value of < 0.001 and then assigned the GO terms and KEGG pathways using the OmicsBox software (BioBam Bioinformatics, Valencia, Spain; https://www.biobam.com/omicsbox/)[62]. In functional enrichment analysis, each set of DEGs was selected as the test set while all other annotated transcripts were considered the reference set. Significantly over-enriched GO terms and KEGG pathways were identified from test set by using one-tailed Fisher's exact test with p-value of < 0.05.

qRT-PCR analysis

To validate the RNA-sequencing data, five $LuxR_{Vs}$-regulon genes were selected and analyzed by qRT-PCR. Total RNAs were extracted from WT-HCD, WT-LCD, and MT-HCD cells as described above. cDNA was synthesized from 1 µg of the total RNA using the iScript cDNA synthesis kit (Bio-Rad, Hercules, CA, USA) in a final volume of 20 µl. qRT-PCR was performed with pairs of specific primers (Supplementary Table S3) and SYBR Green (Bio-Rad) by using the QuantStudio 1 Real-Time PCR System (Thermo Fisher Scientific). The *recA* housekeeping gene was utilized as an internal control gene for normalization, and the relative expression values were calculated using the comparative threshold cycle method ($2^{-\Delta\Delta Ct}$)[63]. The obtained results were presented as means ± standard deviation (SD) from triplicate.

Quantitative comparison of PHA production

To assess PHA biosynthesis, the Nile red agar plate assay was employed as described previously[64]. In the complex medium with 2% agar, which consisted of 10 g of NaCl, 3.7 g of Na_2HPO_4, 1.0 g of KH_2PO_4, 0.5 g of $(NH_4)_2$ HPO_4, 0.2 g of $MgSO_4 \cdot 7H_2O$, 2 ml glycerol, 5 g of bactotryptone, 0.5 g of yeast extract per liter[65] and appropriate antibiotics and arabinose [0.01% (w/v); for the induction of complemented genes], a solution of Nile red in dimethyl sulfoxide was added to achieve a final concentration of 0.5 µg/ml. Wild-type, Δ$luxR_{Vs}$, or the complemented strains were spotted on the plates, and then incubated for 72 h at 27 °C. Subsequently, the intensity of fluorescence from the colonies was observed under UV light. For the quantitative comparison of PHA biosynthesis, the Nile red fluorescence method was used[66]. In brief, the cultures were centrifuged at 12,000 × *g* for 5 min, and the supernatants were discarded. Remaining bacterial cell pellets were then resuspended in 1 ml of distilled water and a solution of Nile red was added to achieve a final concentration of 3.1 µg Nile red per

ml of suspension. After 30 min incubation at dark, second centrifugation was performed and the pellets were resuspended again in 1 ml of distilled water. Finally, the samples were transferred to a 96-well microtiter plate and the fluorescence intensity was measured using the CLARIOstar® Microplate Reader (BMG Labtech, Ortenberg, German) at an excitation wavelength of 535 nm and an emission wavelength of 605 nm. PHA production was quantified by normalizing the fluorescence intensity by optical density at 600 nm (OD_{600}).

Biofilm formation assay

Wild-type, Δ*luxR*$_{Vs}$, and the complemented strains were freshly inoculated into AB-glycerol medium with appropriate antibiotics and arabinose in borosilicate tubes. After static incubation at 27 °C for 72 h, planktonic cells were removed, and their cell density was determined via spectrometric measurement at OD_{595}. Subsequently, the remaining biofilms in the tube were carefully rinsed with phosphate-buffered saline (PBS, pH 7.4) and then stained with 1% (w/v) crystal violet solution for 30 min. After brief washing with distilled water, the biofilm-associated crystal violet was eluted using 100% ethanol and quantified by measuring OD_{550}. The degree of biofilm formation was normalized by dividing OD_{550} by the respective planktonic cell density (OD_{595})[67].

Statistical analysis

Unless noted otherwise, the data presented as means with SD from at least three experiments. Statistical analysis was performed using GraphPad Prism ver. 8.4.3 (GraphPad Software, San Diego, CA, USA; https://www.graphpad.com/), as described in each figure legend.

Data availability

The complete genome sequence of V. scophthalmi 21FBVib0096 strain has been deposited in the GenBank under accession numbers, CP134277 (chromosome 1), CP134278 (chromosome 2), and CP134279 (plasmid). The raw sequencing reads for RNA-sequencing were deposited in the NCBI Short Read Archive (SRA) under accession numbers SRR28019963 to SRR28019971.

Received: 20 July 2024; Accepted: 4 November 2024
Published online: 12 November 2024

References

1. Cai, W., Wang, R. & Zhang, S. Efficient food systems for greater sustainability. *Nat. Food*. **4**, 541–542. https://doi.org/10.1038/s43016-023-00780-3 (2023).
2. Mariutti, L. R. B. et al. The use of alternative food sources to improve health and guarantee access and food intake. *Food Res. Int.* **149**, 110709. https://doi.org/10.1016/j.foodres.2021.110709 (2021).
3. Costello, C. et al. The future of food from the sea. *Nature*. **588**, 95–100. https://doi.org/10.1038/s41586-020-2616-y (2020).
4. KOSIS. Survey on Fishery Production of Fisheries Processing Industry, http://kosis.kr. (2023).
5. Stieglitz, J. D. et al. Advancing production of marine fish in the United States: Olive flounder, *Paralichthys olivaceus*, aquaculture. *J. World Aquacult. Soc.* **52**, 566–581. https://doi.org/10.1111/jwas.12804 (2021).
6. Hwang, J. Y. et al. Current use and management of commercial fish vaccines in Korea. *Fish. Shellfish Immunol.* **102**, 20–27. https://doi.org/10.1016/j.fsi.2020.04.004 (2020).
7. Cho, M. Y. et al. A statistical study on infectious diseases of cultured olive flounder, *Paralichthys olivaceus* in Korea. *J. fish. Pathol.* **21**, 271–278 (2008).
8. Kim, J. W. et al. Statistical data on infectious diseases of cultured olive flounder *Paralichthys olivaceus* from 2005 to 2007. *J. fish. Pathol.* **23**, 369–377 (2010).
9. Sohn, H., Kim, J., Jin, C. & Lee, J. Identification of *Vibrio* species isolated from cultured olive flounder (*Paralichthys olivaceus*) in Jeju Island, South Korea. *Fish. Aquat. Sci.* **22**, 1–8. https://doi.org/10.1186/s41240-019-0129-0 (2019).
10. Qiao, G. et al. Pathogenicity comparison of high- and low-virulence strains of *Vibrio scophthalmi* in olive flounder *Paralichthys olivaceus*. *Fish. Sci.* **79**, 99–109. https://doi.org/10.1007/s12562-012-0567-4 (2013).
11. Cerda-Cuellar, M., Rossello-Mora, R. A., Lalucat, J., Jofre, J. & Blanch, A. *Vibrio scophthalmi* sp. nov., a new species from turbot (*Scophthalmus maximus*). *Int. J. Syst. Bacteriol.* **47**, 58–61. https://doi.org/10.1099/00207713-47-1-58 (1997).
12. Lee, N. S. et al. *Vibrio scophthalmi* infection in Japanese eel *Anguilla japonica* during seawater adaption. *J. fish. Pathol.* **25**, 173–180. https://doi.org/10.7847/jfp.2012.25.3.173 (2012).
13. Qiao, G. et al. Microbiological characteristics of *Vibrio scophthalmi* isolates from diseased olive flounder *Paralichthys olivaceus*. *Fish. Sci.* **78**, 853–863. https://doi.org/10.1007/s12562-012-0502-8 (2012).
14. Azimi, S., Klementiev, A. D., Whiteley, M. & Diggle, S. P. Bacterial quorum sensing during infection. *Annu. Rev. Microbiol.* **74**, 201–219. https://doi.org/10.1146/annurev-micro-032020-093845 (2020).
15. Zhu, J. et al. Quorum-sensing regulators control virulence gene expression in Vibrio cholerae. *Proc. Natl. Acad. Sci. USA*. **99**, 3129–3134. https://doi.org/10.1073/pnas.052694299 (2002).
16. Waters, C. M., Lu, W., Rabinowitz, J. D. & Bassler, B. L. Quorum sensing controls biofilm formation in *Vibrio cholerae* through modulation of cyclic di-GMP levels and repression of *vpsT*. *J. Bacteriol.* **190**, 2527–2536. https://doi.org/10.1128/jb.01756-07 (2008).
17. Miller, M. B. & Bassler, B. L. Quorum sensing in bacteria. *Annu. Rev. Microbiol.* **55**, 165–199. https://doi.org/10.1146/annurev.micro.55.1.165 (2001).
18. Mukherjee, S. & Bassler, B. L. Bacterial quorum sensing in complex and dynamically changing environments. *Nat. Rev. Microbiol.* **17**, 371–382. https://doi.org/10.1038/s41579-019-0186-5 (2019).
19. Henke, J. M. & Bassler, B. L. Three parallel quorum-sensing systems regulate gene expression in *Vibrio harveyi*. *J. Bacteriol.* **186**, 6902–6914. https://doi.org/10.1128/JB.186.20.6902-6914.2004 (2004).
20. Miller, M. B., Skorupski, K., Lenz, D. H., Taylor, R. K. & Bassler, B. L. Parallel quorum sensing systems converge to regulate virulence in *Vibrio cholerae*. *Cell*. **110**, 303–314. https://doi.org/10.1016/s0092-8674(02)00829-2 (2002).
21. Ball, A. S., Chaparian, R. R. & van Kessel, J. C. Quorum sensing gene regulation by LuxR/HapR master regulators in Vibrios. *J. Bacteriol.* **199**, e00105–e00117. https://doi.org/10.1128/JB.00105-17 (2017).
22. Miyamoto, C. M., Chatterjee, J., Swartzman, E., Szittner, R. & Meighen, E. A. The role of *lux* autoinducer in regulating luminescence in *Vibrio harveyi*; control of *luxR* expression. *Mol. Microbiol.* **19**, 767–775. https://doi.org/10.1046/j.1365-2958.1996.417948.x (1996).

23. Jobling, M. G. & Holmes, R. K. Characterization of *hapR*, a positive regulator of the *Vibrio cholerae* HA/protease gene *hap*, and its identification as a functional homologue of the *Vibrio harveyi luxR* gene. *Mol. Microbiol.* **26**, 1023–1034. https://doi.org/10.1046/j.1365-2958.1997.6402011.x (1997).
24. McDougald, D., Rice, S. A. & Kjelleberg, S. The marine pathogen *Vibrio vulnificus* encodes a putative homologue of the *Vibrio harveyi* regulatory gene, *luxR*: a genetic and phylogenetic comparison. *Gene.* **248**, 213–221. https://doi.org/10.1016/s0378-1119(00)00117-7 (2000).
25. Garcia-Aljaro, C., Eberl, L., Riedel, K. & Blanch, A. R. Detection of quorum-sensing-related molecules in *Vibrio scophthalmi*. *BMC Microbiol.* **8**, 138. https://doi.org/10.1186/1471-2180-8-138 (2008).
26. Garcia-Aljaro, C., Melado-Rovira, S., Milton, D. L. & Blanch, A. R. Quorum-sensing regulates biofilm formation in *Vibrio scophthalmi*. *BMC Microbiol.* **12**, 287. https://doi.org/10.1186/1471-2180-12-287 (2012).
27. Kim, Y. et al. Crystal structure of SmcR, a quorum-sensing master regulator of *Vibrio vulnificus*, provides insight into its regulation of transcription. *J. Biol. Chem.* **285**, 14020–14030. https://doi.org/10.1074/jbc.M109.100248 (2010).
28. Chaparian, R. R., Ball, A. S. & van Kessel, J. C. Hierarchical Transcriptional Control of the LuxR Quorum-Sensing Regulon of *Vibrio harveyi*. *J. Bacteriol.* **202**, https://doi.org/10.1128/JB.00047-20 (2020).
29. Kim, B. S. et al. QStatin, a Selective Inhibitor of Quorum Sensing in *Vibrio* Species. *mBio* 9, (2018). https://doi.org/10.1128/mbio.02262 – 02217 https://doi.org:10.1128/mBio.02262-17.
30. Kalburge, S. S., Carpenter, M. R., Rozovsky, S. & Boyd, E. F. Quorum Sensing Regulators Are Required for Metabolic Fitness in *Vibrio parahaemolyticus*. *Infect. Immun.* **85**, https://doi.org/10.1128/IAI.00930-16 (2017).
31. Cai, J. et al. Differential binding of LuxR in response to temperature gauges switches virulence gene expression in *Vibrio alginolyticus*. *Microbiol. Res.* **263**, 127114. https://doi.org/10.1016/j.micres.2022.127114 (2022).
32. Lu, J. N., Tappel, R. C. & Nomura, C. T. Mini-review: biosynthesis of poly(hydroxyalkanoates). *Polym. Rev.* **49**, 226–248. https://doi.org/10.1080/15583720903048243 (2009).
33. Choi, S. Y. et al. Microbial polyhydroxyalkanoates and Nonnatural Polyesters. *Adv. Mater.* **32**, e1907138. https://doi.org/10.1002/adma.201907138 (2020).
34. Bordas, M. A., Balebona, M. C., Zorrilla, I., Borrego, J. J. & Morinigo, M. A. Kinetics of adhesion of selected fish-pathogenic *Vibrio* strains of skin mucus of gilt-head sea bream (*Sparus aurata L*). *Appl. Environ. Microbiol.* **62**, 3650–3654. https://doi.org/10.1128/aem.62.10.3650-3654.1996 (1996).
35. Bourassa, L. & Camilli, A. Glycogen contributes to the environmental persistence and transmission of *Vibrio cholerae*. *Mol. Microbiol.* **72**, 124–138. https://doi.org/10.1111/j.1365-2958.2009.06629.x (2009).
36. Elser, J. J., Stabler, L. B. & Hassett, R. P. Nutrient limitation of bacterial growth and rates of bacterivory in lakes and oceans: a comparative study. *Aquat. Microb. Ecol.* **9**, 105–110 (1995).
37. Mitra, R., Xu, T., Chen, G. Q., Xiang, H. & Han, J. An updated overview on the regulatory circuits of polyhydroxyalkanoates synthesis. *Microb. Biotechnol.* **15**, 1446–1470. https://doi.org/10.1111/1751-7915.13915 (2022).
38. Sun, W., Cao, J. G., Teng, K. & Meighen, E. A. Biosynthesis of poly-3-hydroxybutyrate in the luminescent bacterium, *Vibrio harveyi*, and regulation by the lux autoinducer, N-(3-hydroxybutanoyl)homoserine lactone. *J. Biol. Chem.* **269**, 20785–20790 (1994).
39. Li, H. F., Tian, L., Lian, G., Fan, L. H. & Li, Z. J. Engineering *Vibrio alginolyticus* as a novel chassis for PHB production from starch. *Front. Bioeng. Biotechnol.* **11**, 1130368. https://doi.org/10.3389/fbioe.2023.1130368 (2023).
40. Li, H. H. et al. Nonsterilized Fermentation of Crude Glycerol for Polyhydroxybutyrate Production by Metabolically Engineered *Vibrio natriegens*. *ACS Synth. Biol.* **12**, 3454–3462. https://doi.org/10.1021/acssynbio.3c00498 (2023).
41. Zhang, M. et al. QsvR and OpaR coordinately repress biofilm formation by *Vibrio parahaemolyticus*. *Front. Microbiol.* **14**, 1079653. https://doi.org/10.3389/fmicb.2023.1079653 (2023).
42. Gregory, G. J. & Boyd, E. F. Stressed out: bacterial response to high salinity using compatible solute biosynthesis and uptake systems, lessons from Vibrionaceae. *Comput. Struct. Biotechnol. J.* **19**, 1014–1027. https://doi.org/10.1016/j.csbj.2021.01.030 (2021).
43. Gregory, G. J., Morreale, D. P., Carpenter, M. R., Kalburge, S. S. & Boyd, E. F. Quorum sensing regulators AphA and OpaR control expression of the Operon responsible for biosynthesis of the compatible Solute Ectoine. *Appl. Environ. Microbiol.* **85**, e01543–e01519. https://doi.org/10.1128/AEM.01543-19 (2019).
44. Gnanagobal, H. & Santander, J. Host-Pathogen interactions of Marine Gram-positive Bacteria. *Biology*. **11**, 1316. https://doi.org/10.3390/biology11091316 (2022).
45. Hossain, A. et al. Antibiotics, antibiotic-resistant bacteria, and resistance genes in aquaculture: risks, current concern, and future thinking. *Environ. Sci. Pollut Res. Int.* **29**, 11054–11075. https://doi.org/10.1007/s11356-021-17825-4 (2022).
46. Greenberg, E., Hastings, J. W. & Ulitzur, S. Induction of luciferase synthesis in *Beneckea harveyi* by other marine bacteria. *Arch. Microbiol.* **120**, 87–91. https://doi.org/10.1007/BF00409093 (1979).
47. Kang, S. & Lee, K. H. Transition of Dephospho-DctD to the Transcriptionally Active State via Interaction with Dephospho-IIA(Glc). *mBio* 13, e0383921 (2022). https://doi.org/10.1128/mbio.03839-21
48. Wick, R. R., Judd, L. M., Gorrie, C. L., Holt, K. E. & Unicycler Resolving bacterial genome assemblies from short and long sequencing reads. *Plos Comput. Biol.* **13**, e1005595. https://doi.org/10.1371/journal.pcbi.1005595 (2017).
49. Hyatt, D. et al. Prodigal: prokaryotic gene recognition and translation initiation site identification. *BMC Bioinform.* **11**, 119. https://doi.org/10.1186/1471-2105-11-119 (2010).
50. Lowe, T. M. & Chan, P. P. tRNAscan-SE On-line: integrating search and context for analysis of transfer RNA genes. *Nucleic Acids Res.* **44**, W54–57. https://doi.org/10.1093/nar/gkw413 (2016).
51. Nawrocki, E. P. et al. Rfam 12.0: updates to the RNA families database. *Nucleic Acids Res.* **43**, D130–137. https://doi.org/10.1093/nar/gku1063 (2015).
52. Edgar, R. C. PILER-CR: fast and accurate identification of CRISPR repeats. *BMC Bioinform.* **8**, 18. https://doi.org/10.1186/1471-2105-8-18 (2007).
53. Bland, C. et al. CRISPR recognition tool (CRT): a tool for automatic detection of clustered regularly interspaced palindromic repeats. *BMC Bioinform.* **8**, 209. https://doi.org/10.1186/1471-2105-8-209 (2007).
54. Powell, S. et al. eggNOG v4.0: nested orthology inference across 3686 organisms. *Nucleic Acids Res.* **42**, D231–239. https://doi.org/10.1093/nar/gkt1253 (2014).
55. Kanehisa, M. & Goto, S. KEGG: kyoto encyclopedia of genes and genomes. *Nucleic Acids Res.* **28**, 27–30. https://doi.org/10.1093/nar/28.1.27 (2000).
56. Overbeek, R. et al. The SEED and the Rapid Annotation of microbial genomes using Subsystems Technology (RAST). *Nucleic Acids Res.* **42**, D206–214. https://doi.org/10.1093/nar/gkt1226 (2014).
57. Edgar, R. C. Search and clustering orders of magnitude faster than BLAST. *Bioinformatics*. **26**, 2460–2461. https://doi.org/10.1093/bioinformatics/btq461 (2010).
58. Kim, B. S. et al. MARTX Toxin-Stimulated Interplay between Human Cells and *Vibrio vulnificus*. *mSphere* 5, (2020). https://doi.org/10.1128/msphere. 00659 – 00620 https://doi.org:10.1128/mSphere.00659-20.
59. Lim, J. G., Bang, Y. J. & Choi, S. H. Characterization of the *Vibrio vulnificus* 1-Cys peroxiredoxin Prx3 and regulation of its expression by the Fe-S cluster regulator IscR in response to oxidative stress and iron starvation. *J. Biol. Chem.* **289**, 36263–36274. https://doi.org/10.1074/jbc.M114.611020 (2014).

60. Robinson, M. D., McCarthy, D. J. & Smyth, G. K. edgeR: a Bioconductor package for differential expression analysis of digital gene expression data. *Bioinformatics*. **26**, 139–140. https://doi.org/10.1093/bioinformatics/btp616 (2010).
61. Robinson, M. D. & Oshlack, A. A scaling normalization method for differential expression analysis of RNA-seq data. *Genome Biol.* **11**, R25. https://doi.org/10.1186/gb-2010-11-3-r25 (2010).
62. Gotz, S. et al. High-throughput functional annotation and data mining with the Blast2GO suite. *Nucleic Acids Res.* **36**, 3420–3435. https://doi.org/10.1093/nar/gkn176 (2008).
63. Livak, K. J. & Schmittgen, T. D. Analysis of relative gene expression data using real-time quantitative PCR and the 2(-Delta Delta C(T)) method. *Methods*. **25**, 402–408. https://doi.org/10.1006/meth.2001.1262 (2001).
64. Spiekermann, P., Rehm, B. H., Kalscheuer, R., Baumeister, D. & Steinbuchel, A. A sensitive, viable-colony staining method using Nile red for direct screening of bacteria that accumulate polyhydroxyalkanoic acids and other lipid storage compounds. *Arch. Microbiol.* **171**, 73–80. https://doi.org/10.1007/s002030050681 (1999).
65. Sasidharan, R. S., Bhat, S. G. & Chandrasekaran, M. Biocompatible polyhydroxybutyrate (PHB) production by marine *Vibrio azureus* BTKB33 under submerged fermentation. *Ann. Microbiol.* **65**, 455–465. https://doi.org/10.1007/s13213-014-0878-z (2015).
66. Zuriani, R., Vigneswari, S., Azizan, M. N. M., Majid, M. I. A. & Amirul, A. A. A high throughput Nile red fluorescence method for rapid quantification of intracellular bacterial polyhydroxyalkanoates. *Biotech. Bioprocess. Eng.* **18**, 472–478. https://doi.org/10.1007/s12257-012-0607-z (2013).
67. Kim, H. S., Lee, M. A., Chun, S. J., Park, S. J. & Lee, K. H. Role of NtrC in biofilm formation via controlling expression of the gene encoding an ADP-glycero-manno-heptose-6-epimerase in the pathogenic bacterium, *Vibrio vulnificus*. *Mol. Microbiol.* **63**, 559–574. https://doi.org/10.1111/j.1365-2958.2006.05527.x (2007).
68. Simon, R., Priefer, U. & Pühler, A. A. Broad Host Range Mobilization System for *in Vivo* Genetic Engineering: Transposon Mutagenesis in Gram negative Bacteria. *Nat. Biotech.* **1**, 784–791. https://doi.org/10.1038/nbt1183-784 (1983).
69. Philippe, N., Alcaraz, J. P., Coursange, E., Geiselmann, J. & Schneider, D. Improvement of pCVD442, a suicide plasmid for gene allele exchange in bacteria. *Plasmid*. **51**, 246–255. https://doi.org/10.1016/j.plasmid.2004.02.003 (2004).

Acknowledgements

We thank all the members of the Molecular Food Microbiology and Toxinology Laboratory at Ewha Womans University for their technical assistance and helpful discussion. This research was supported by the National Institute of Fisheries Science, Ministry of Oceans and Fisheries, Korea (R2022076). This research was also supported by the Korea government (MSIT) (RS-2023-00280142).

Author contributions

B.S. and B.S.K. designed the experiments, B.S. performed the experiments, B.S. and B.S.K. interpreted the data, M.S.K. and B.S.K. acquired critical reagents and funding. B.S. and B.S.K. wrote original draft and all authors reviewed and edited the manuscript.

Declarations

Competing interests

The authors declare no competing interests.

Additional information

Supplementary Information The online version contains supplementary material available at https://doi.org/10.1038/s41598-024-78803-7.

Correspondence and requests for materials should be addressed to B.S.K.

Reprints and permissions information is available at www.nature.com/reprints.

Publisher's note Springer Nature remains neutral with regard to jurisdictional claims in published maps and institutional affiliations.

Open Access This article is licensed under a Creative Commons Attribution-NonCommercial-NoDerivatives 4.0 International License, which permits any non-commercial use, sharing, distribution and reproduction in any medium or format, as long as you give appropriate credit to the original author(s) and the source, provide a link to the Creative Commons licence, and indicate if you modified the licensed material. You do not have permission under this licence to share adapted material derived from this article or parts of it. The images or other third party material in this article are included in the article's Creative Commons licence, unless indicated otherwise in a credit line to the material. If material is not included in the article's Creative Commons licence and your intended use is not permitted by statutory regulation or exceeds the permitted use, you will need to obtain permission directly from the copyright holder. To view a copy of this licence, visit http://creativecommons.org/licenses/by-nc-nd/4.0/.

© The Author(s) 2024